Stress evolution in platinum thin films during low-energy ion irradiation

Wai-Lun Chan,[1] Kai Zhao,[1] Nhon Vo,[1] Yinon Ashkenazy,[2] David G. Cahill,[1] and Robert S. Averback[1]
[1]*Department of Materials Science and Engineering, University of Illinois at Urbana-Champaign, Urbana, Illinois 61801, USA*
[2]*Racah Institute of Physics, Hebrew University of Jerusalem, 91904 Jerusalem, Israel*
(Received 18 August 2007; revised manuscript received 3 March 2008; published 5 May 2008)

Stress evolution of Pt thin films during low-energy ion irradiation is investigated by using wafer bending measurements and molecular dynamics simulations. Noble gas ions ranging in mass from He to Xe and energy from 0.5 to 5 keV are used. Depending on the type and energy of the ion, the change in stress can either be tensile or compressive. Heavier or higher-energy ions tend to create tensile stress, while lighter ions such as He always induce compressive stress. The stress evolution also depends on the initial state of stress in the thin films. The results are explained by a competition between the tensile stress induced by local melting along the ion track and the compressive stress induced by the accumulation of ion-induced interstitials in defect clusters or grain boundaries, often beyond the calculated ion penetration depth. Anisotropic diffusion of interstitials under an external stress field also plays an important role in the stress evolution. Molecular dynamics simulation is employed to evaluate the importance of each of these microscopic mechanisms.

DOI: 10.1103/PhysRevB.77.205405 PACS number(s): 61.80.Jh, 62.25.−g, 81.40.Wx, 68.47.De

I. INTRODUCTION

The effects of ion irradiation on materials have been studied for many years. While a majority of these investigations were initially concerned with ion implantation,[1] defect production,[2] and sputtering,[3] newer interests have evolved in the areas of ion beam induced patterning and self-organization. These include ripple and dot formation,[4] dewetting,[5] and compositional patterning in bulk[6] and on the surface.[7] Local stress in the film is frequently an important driving force for self-organization.[8] Since large stresses can be induced during irradiation, several recent studies have considered that the ion-induced stress can be a possible driving force for pattern formation on irradiated surfaces.[9–11] In addition, irradiation-induced stress has also been used as a way to control the shape of thin film structures in microelectromechanical system devices,[12] and ion beams have been increasingly used as processing tools in preparing nanostructures and smoothing surfaces.[1,4] Knowing the stress distribution and the mechanisms that induce the stress becomes critical in advancing these applications. However, little is known about irradiation-induced stresses, particularly for metal surfaces irradiated by low-energy ions. These stresses can derive from a number of sources, irradiation-induced point defects and defect clusters, adatoms and their clusters, and the inclusion of the implanted ions. The present work is an initial investigation of stress that is developed in thin metal films irradiated by low-energy ions.

Pervious works on irradiation-induced stress have primarily employed high-energy ions.[13–18] Since the low-energy beams have a much shallower implantation range than the high-energy beams, effects from surface defects and diffusion of ion-induced bulk defects beyond the implantation range can have a far more dominant role for the low-energy ions. Irradiation-induced stress due to low-energy ions have been studied on materials, such as Si (Ref. 19) and SiO_2,[20] but for metals, only Cu has been studied.[21,22] In the work on Cu, it was found that in steady state, the stresses are compressive and on the order of a few gigapascals. The origin of these stresses and their subsequent evolution was attributed to the incorporation of the gas ions[21] and the subsequent evolution of ion-induced interstitials and vacancies.[22] These studies, however, did not explore the complexity that is usually found in the defect evolution of irradiated materials. Multiple atomistic processes, such as the initial melting around the ion track, diffusion, recombination, and nucleation of extended defects, and the interaction of the inert gas ions with defects can all contribute to changes in stress, but previous studies have not explored these different processes. Second, most previous work has assumed that the changes in stress were generated within the implantation depth of the ions. This assumption is reasonable for high-energy ions, but for low-energy ions, the typical implantation depth is less than 5 nm and the diffusion of ion-induced defects (e.g., interstitials) can significantly broaden the stress distribution.

In order to differentiate the effects from different ion-induced atomistic processes, in the present work, we have systematically investigated how the stress evolution in Pt thin films depends on the ion energy, ion species, initial stress, and film thickness. Thin film samples are chosen such that we can control the initial film stress by varying the growth conditions. In addition, experiments on thin films with different thicknesses enable us to determine the range of different atomistic processes that induce the stress and the depth distribution of the ion-induced stress. While the study is predominantly experimental, we employ molecular dynamics (MD) simulations to evaluate different mechanisms of stress generation, including (i) the stresses associated with various types of defects and defect clusters, (ii) defect production by the various ions, and (iii) the anisotropic diffusivity of interstitials in highly stressed thin films.

Our results show that the evolution of stress depends on the mass of ions. For light ions such as He, the stress becomes increasingly compressive with dose, and it does not reach a saturation stress up to 1×10^{16} cm^{-2}. This stress is mainly induced by gas incorporation and possibly by interstitial loops created by the gas ions. In contrast, the initial stress produced by heavy ions such as Xe is tensile, and the tensile stress ceases to increase at a much lower dose,

 ©2008 The American Physical Society

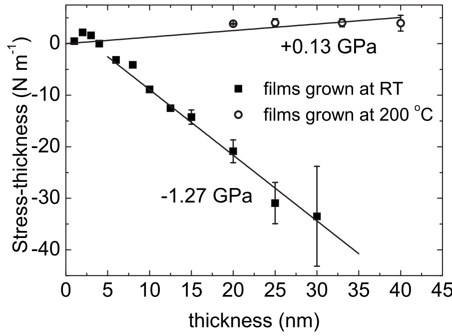

FIG. 1. The stress thickness of Pt films grown on Si cantilevers as a function of film thickness. Two different growth temperatures are used. The slope of the curve gives the average initial stress of the films. Data points with error bars represent the average over three or more individual growths.

$\sim 10^{14}$ cm^{-2}. We attribute this behavior to thermal spikes created by heavy ions. Another significant finding in this work is that the irradiation-induced stress depends rather sensitively on the initial state of stress in the Pt thin films. For example, during Ar irradiation, compressive stress is induced in a film having nearly zero initial stress, but tensile stress is induced in a film that is initially compressive. Lastly, we show by using Pt films of different thicknesses and by switching ion energies during irradiation that the induced stresses extend well beyond the implantation depth of the ions.

The remainder of this paper will be arranged as follows. First, we describe our experimental methods and the state of stress in the as-prepared Pt thin films. We then show the evolution of stress during irradiation obtained by using an *in situ* curvature measurement technique. This is followed by the results of the MD simulations. In Sec. V, we provide a comprehensive picture to explain the wide range of behaviors obtained in the experiments.

II. EXPERIMENTAL METHODS

Pt films ranging in thickness from 15 to 40 nm were grown on 2–2.5 μm thick and 450 μm long Si(001) cantilevers by using sputter deposition. The actual thickness of each sample is determined by scanning electron microscopy. The base pressure of the deposition chamber was 5×10^{-8} Torr. During deposition, the pressure was raised to 3×10^{-3} Torr by feeding Ar gas into the chamber. By increasing the growth temperature from room temperature (RT) to 200 °C, the initial stress of the film at RT changed from highly compressive to slightly tensile (see Fig. 1). For the films that were deposited at elevated temperature, the Si cantilevers were first oxidized at 1000 °C for 3 h before deposition. This procedure yields a layer of thermally grown oxide of 110 nm and thus prevents diffusion of Si into the Pt films and the formation of platinum silicide.[23] After deposition, the samples were immediately transferred to the irradiation chamber, which has a base pressure of 1×10^{-8} Torr. During the transfer, samples were exposed to air for less than 1 h. Control experiments were also performed on films that were grown *in situ* in the irradiation chamber. The results show no significant differences.

All ion irradiations were performed at RT. The incidence angle of the beam was 20° from the surface normal; ion fluxes ranged from 2×10^{11} to 5×10^{12} cm^{-2} s^{-1}. The ion flux was determined by placing a Faraday cup at the position of the sample. During the ion bombardment process, the curvature of the cantilever was monitored *in situ* by using a scanning laser beam. The details of the measurement technique can be found elsewhere.[24] We point out here, however, that since the Si wafers are only 2 μm thick, the technique is highly sensitive to stress in the films. The curvature is measured in a direction parallel to the projection of the ion beam on the sample surface. The in-plane stress σ of the film with respect to time can be related to the substrate curvature κ by the Stoney equation,[25]

$$S(t) = \int_0^h \sigma(z,t)dz = \frac{M_s h_s^2}{6}\kappa(t), \tag{1}$$

where z is the direction normal to the surface, h is the thickness of the Pt film, and h_s and M_s are the thickness and biaxial modulus of the substrate, respectively. The biaxial modulus for Si(001) is 180.5 GPa. Note that the total integrated stress (or stress thickness) S in Eq. (1) includes the contribution from both the initial stress of the Pt film and the change in stress induced by the irradiation process. In the following discussion, we will concentrate on the change in stress thickness as a function of time during ion irradiation, $\Delta S(t) = S(t) - S(0)$.

We can estimate the temperature rise during ion irradiation by solving the heat diffusion equation. For our sample geometry and ion beam parameters, the temperature increase contributed by ion irradiation is expected to be less than 0.04 K for the highest flux and energy used. The steady-state temperature rise created by the measurement laser is about 3 K. The estimated change in stress thickness induced by the temperature rise (due to thermal mismatch between films and substrate) is less than 0.2 N m^{-1} even for our thickest samples, which is negligible in our measurements.

A. Initial stress and microstructure of the Pt films

Before presenting our results on irradiation-induced stress, we consider the initial stress of the as-deposited films. Figure 1 shows the initial stress thickness in Pt films as a function of thickness. The positive direction, here and throughout, denotes tensile stress. The stress as a function of thickness is given by the local slope of the curve. Two growth temperatures are used. Films grown at RT show a tensile stress in the first 3 nm. The stress then turns compressive as the film becomes thicker, and it maintains a steady-state value of -1.27 GPa. This magnitude of stress is typical for Pt thin films grown by using sputter deposition.[26] The second group of films, which are grown at 200 °C, are slightly tensile for the first 25 nm and the total stress thickness essentially remains unchanged when the thickness increases from 25 to 40 nm. The average stress in the films grown at 200 °C is 0.1–0.2 GPa (tensile) at various film thicknesses. Since the initial stress of the films grown at

200 °C is small compared to the change in film stress during irradiation, we do not delineate the slight differences in the film stress at different thicknesses. This group of films will be referred to as slightly tensile films with an average stress of 0.13 ± 0.04 GPa.

Atomic force microscopy shows that both sets of film are continuous. The rms roughnesses are 0.12 and 0.37 nm over a 1×1 μm^2 area for a 30 nm film deposited at RT and 200 °C, respectively. After the sample is irradiated by 4 keV Ar with a fluence of 10^{16} cm^{-2}, the resultant rms roughness for the two groups of films becomes 1.1 and 1.7 nm, respectively. Mounds with sizes ranging from 10 to 50 nm are developed on the surface after irradiation, but no self-organized features or anisotropy is observed in the surface morphology. X-ray analysis indicates that both sets of samples have a similar microstructure; they have (111) textures, while the grain size is 12 nm for a 40 nm thick film grown at 200 °C and 9 nm for a 30 nm thick film grown at RT. The average grain size only slightly increases with increasing film thickness. A 25 nm thick film grown at 200 °C, for example, has a grain size of 11 nm, which is only slightly smaller than the 40 nm film grown under the same conditions. These results indicate that the films have columnar grain structures. Rutherford backscattering measurements on the films deposited at high temperature show no indications of silicide formation at the Pt/SiO_2 interface or diffusion of Si into Pt.

III. RESULTS FROM IRRADIATION EXPERIMENTS

A. Ion-induced stress in highly compressive Pt films

Figure 2(a) shows the change in the stress thickness (ΔS) as a function of ion dose for Pt films that are irradiated with Ar ions with different energies (1–4 keV). The samples are Pt films grown at RT with an initial stress of -1.27 GPa. The ion flux used is 1×10^{12} cm^{-2} s^{-1}. The curves show a rapid rise in tensile stress for ion doses less than 5×10^{14} cm^{-2} and a smaller steady increase beyond that. The rise in stress is more rapid and the integrated stress is larger for the higher-energy ions. The steady-state increase in tensile stress at high doses presumably derives from the sputter removal of the compressive Pt. The dotted lines in Fig. 2(a), for example, show the expected changes in stress thickness due to sputtering. The sputter yields were estimated by using SRIM.[27] Except for the sample irradiated by 1 keV Ar, the slopes of the measured curves appears to asymptotically fall on the calculated slope. The reason for the deviation in the data obtained from 1 keV Ar is unknown. Nevertheless, it is reasonable to claim that for doses larger than 10^{15} cm^{-2}, the damage created by the ions saturates and the change in stress arises mainly from the removal of the compressive Pt film. We have also carried out the experiments by using different ion fluxes, and for fluxes ranging from 2×10^{11} to 5×10^{12} cm^{-2} s^{-1}, ΔS is only a function of dose. The results are also independent of the initial film thickness within the range studied, i.e., 15–30 nm.

Results for the changes in stress in Pt films bombarded by different ions, 2 keV Xe, Ar, and Ne, and 0.5 keV He, are shown in Fig. 2(b). The films bombarded by Xe, Ar, and Ne

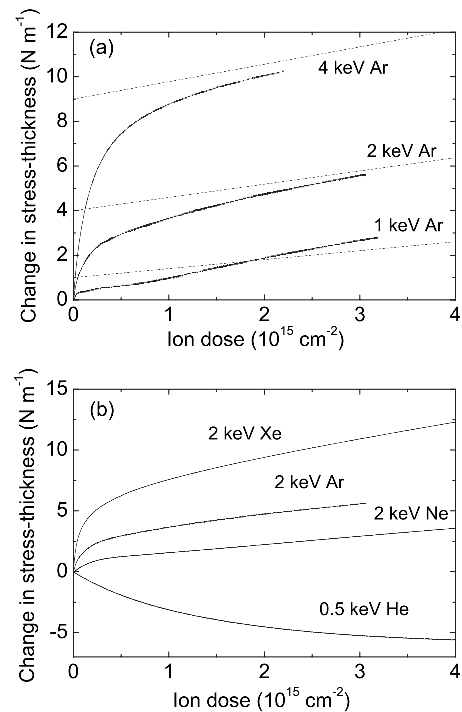

FIG. 2. (a) The change in the stress thickness of Pt films during ion irradiation. These samples have a strong initial biaxial compressive stress of 1.27 GPa. The dotted lines on the graph represent the expected change in the stress thickness due to the sputtering of the highly compressive film. (b) The change in the stress thickness of the highly compressive films irradiated by different ions. Films with thickness from 15 to 30 nm are used in (a) and (b). For these highly compressive films, the stress evolution is independent of the film thickness.

show similar behaviors: a rapid increase in tensile stress at low doses and a smaller constant change in stress with dose at higher doses. If we assume, for the moment, that the changes in stress are concentrated within the range of the ions, a tensile stress of $\approx 2-3$ GPa is derived for the case of Xe. For 2 keV Ne, the initial compressive stress thickness is reduced by the tensile change in the bombarded region, but the integral stress in the film, nevertheless, remains compressive. Since the range of Ne ions is greater than those of Ar and Xe, the average increase in tensile stress in the damaged region is thus significantly larger for the film bombarded by heavier ions. As we discuss below, our results show that the mechanism creating the tensile stress in Pt correlates with the damage energy density, and not the damage energy or ion range.

Bombardment with He ions shows a qualitatively different behavior. A monotonically increasing compressive stress is induced in the film from the outset of the irradiation. This behavior is similar to the earlier observation in Cu bombarded by He.[21] The result is perhaps not too surprising for Pt since He ions have a very low damage energy in Pt and the energy transfer from He to Pt atoms is low. SRIM (Ref. 27) shows, in fact, that for energies less than ≈ 1 keV, essentially no defects are created during implantation.

Finally, no significant stress relaxation is observed after the irradiation is stopped, except for films bombarded by He

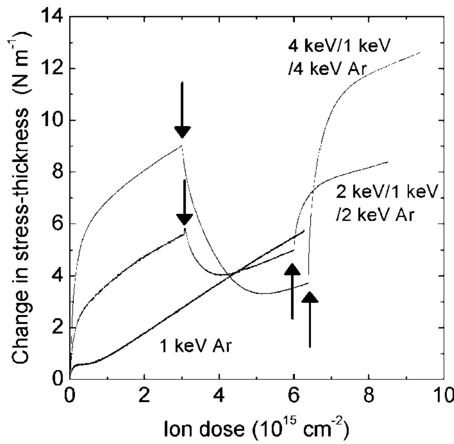

FIG. 3. The stress evolution of the highly compressive films irradiated by switching between different energy ions. The arrows on the graph represent the instance when the ion energy is changed. The uppermost and the middle curve represent the switching between 4/1/4 keV Ar and 2/1/2 keV Ar, respectively. The change in stress thickness of a film bombarded by 1 keV Ar is shown for comparison. The initial film thickness is 15 nm.

and Ne for which there is a small tensile rise (<1 N m^{-1}) in the stress thickness. The damage responsible for the change in stress is thus relatively stable at room temperature, which is consistent with the fact that most bulk diffusion processes, except interstitial diffusion, are not activated in Pt at room temperature. Vacancies, for example, do not become mobile until ≈ 300 °C.[28] Interstitials, on the other hand, diffuse so fast that they rapidly incorporate into stable sites. Hence, diffusion of isolated interstitials will not contribute to stress relaxation after the irradiation has ended.

B. Switching between different energy ions

To explore the interactions of the ions with the existing damage in the film, we change the ion energy after the films have been irradiated to a dose of $\approx 3\times 10^{15}$ cm^{-2}. This set of experiments is performed on the initially compressive Pt films. The results are shown in Fig. 3. The arrows on the curve indicate the doses where we change the ion energy. The upper solid curve shows the evolution of the stress thickness for a film bombarded first by 4 keV Ar, then by 1 keV Ar, and then again by 4 keV Ar. The lower solid curve shows the changes in stress for the switching between 2 keV Ar, 1 keV Ar, and 2 keV Ar. The change in stress thickness of a film bombarded only with 1 keV Ar is shown in Fig. 3 for comparison.

When we switch the Ar ion beam from high to low energies, a strong recovery of the compressive stress is observed. For both 4 and 2 keV Ar, the stress thicknesses drop to new levels, which are comparable to the 1 keV irradiation alone; this occurs within a dose of $\approx 2\times 10^{15}$ cm^{-2} after changing the energy. Notably, both the absolute and relative recoveries are greater following the 4 keV irradiation. Similarly, the stress thickness after 1 keV irradiation alone is greater (more tensile) than that when the 1 keV irradiation follows the 2 and 4 keV irradiations. These experiments illustrate first that

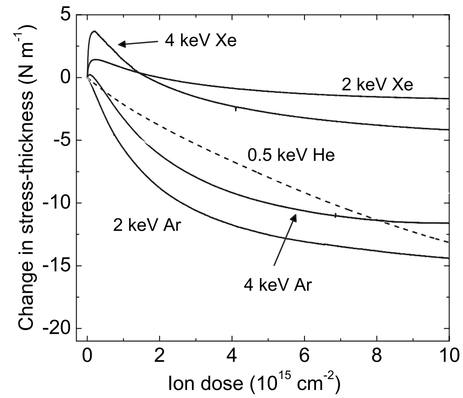

FIG. 4. The evolution of the stress thickness of films irradiated by different ions. These samples have a small initial tensile stress of 0.13 GPa and the initial film thickness is 40 nm.

the damage produced by different energy ions is not simply linearly proportional to the deposited damage energy, and second, that the 1 keV Ar interacts with existing damage well beyond the 1 keV implantation depth.

These conclusions will be discussed in detail below; however, we point out here that the recovery of the compressive stress after switching to the lower-energy irradiation cannot be due to sputtering alone. This can be realized by calculating the incremental stress using the slope of the stress-thickness curve, as a function of Pt removed after switching to 1 keV Ar. If sputtering alone was responsible for the change in stress thickness, the incremental stress obtained from the slope of the curves represents the stress of the film being sputtered. For the 4-1-4 keV curve, this calculated stress is in the range of 10–30 GPa, within a dose of 1×10^{15} cm^{-2} after the switching of the ion energy. This incremental stress is far too large to be the stress in the film, which should be, at most, in the range of 1–2 GPa. Therefore, sputtering cannot account for a large fraction of the stress change when we switch to lower-energy ions.

When we switch back to the higher-energy ions, tensile stress is restored at nearly the same rate as when it was initially introduced at $t=0$, suggesting that the same microscopic processes are at play. The high "reversibility" in the change in stress also precludes any irreversible mechanism such as grain growth or grain boundary relaxation as important factors in the stress evolution.

C. Ion-induced stress in tensile Pt films

Similar experiments were performed on the Pt films having a low value of initial tensile stress (0.1–0.2 GPa). Figure 4 shows the results for these films bombarded by 0.5 keV He, 2 keV Ar, 4 keV Ar, 2 keV Xe, and 4 keV Xe at RT. The initial thickness of these films is 40 nm. The stress evolution in these films is remarkably different from that in the compressive films. For the bombardment with 2 keV Ar, for example, we observe a compressive change in the stress thickness, which is in contrast to the tensile stress observed in the highly compressive Pt films. For 4 keV Ar and Xe, we still observe an initial increase in the tensile stress, but this quickly saturates and the change soon turns compressive. At

doses larger than 5×10^{15} cm^{-2}, the stress thickness has become negative and a steady state is reached where additional changes in stress are due to sputter removal of the initially tensile Pt layer. Notice the difference in the slopes at high doses between these samples and those for the compressive films in Fig. 2. The appearance of a peak in 4 keV Ar and Xe indicates that at least two competing mechanisms with different time scales are responsible for the observed behaviors. The dose that produces the tensile rise in Fig. 4 is similar to the dose that produces the tensile rise observed in highly compressive Pt, which suggests that the same mechanism is responsible for the tensile change in both types of films. The process responsible for the compressive stress, however, saturates at a much higher dose ($\sim5\times10^{15}$ cm^{-2}). For He irradiation, the stress-thickness decreases monotonically with dose.

If we assume that all the stress change occurs within the damaging depth of the ions, we can determine the average stress σ_{av} in the damaged layer of thickness h_{ion} as a function of dose. After subtracting the contribution due to sputtering, the stress as a function of dose Φ can be expressed as

$$\sigma_{av}(\Phi) = \frac{\Delta S - \sigma_i v \Phi / f}{h_{ion}} + \sigma_i. \tag{2}$$

In this expression, v is the erosion velocity of the surface, f is the ion flux, and σ_i is the initial stress of the film. By using Eq. (2), we attempt to determine the steady-state stress (for $\Phi>5\times10^{15}$ cm^{-2}) for films bombarded by 2 keV Ar by using the assumption $h_{ion}=2.2$ nm. This value of h_{ion} represents twice the centroid of the damage energy distribution calculated in SRIM, which is consistent with the value observed in the MD simulations.[29] The value v is calculated from the sputter yield obtained in SRIM and σ_i is determined from the curvature of the cantilever before sputtering. Even though the sputter yield obtained by SRIM may not correspond to the exact sputter yield for our samples, this does not introduce a significant error to our estimate because ΔS is around an order of magnitude larger than $\sigma_i v \Phi / f$. For the strongly compressive film, we obtain a steady-state stress ≈1 GPa. For the slightly tensile film, we obtain a steady-state stress ≈-6 GPa. Immediately, we find two inconsistencies. First, the initially tensile film becomes compressive in steady state but the initially compressive film becomes tensile. Even though the two films may have different stresses in steady state, the initially tensile film should not become more compressive than the initially compressive film. Second, the compressive stress developed in the films grown at 200 °C is high compared to the yield stress that we expect in Pt thin films: a recent nanoindentation experiment shows that the maximum shear stress in Pt is 4.4 GPa,[30] which is comparable to the 6 GPa determined by Eq. (2).

The likely explanation for this behavior is that the compressive stress is generated at a depth beyond the range of the ions. This hypothesis is consistent with the stress recovery presented in Sec. III B, in which the stress located beyond the range of the (1 keV Ar) ion can be relaxed. In this case, however, the damaged region beyond the range of ions is undamaged, whereas in Sec. III B, the region was first damaged by higher-energy ions. In addition, interstitial atoms, which generate compressive stress, are mobile at room temperature and can migrate deeper into the sample.

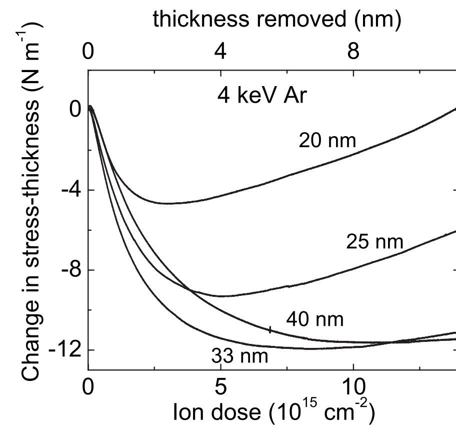

FIG. 5. The change in stress thickness of the slightly tensile films bombarded by 4 keV Ar as a function of ion dose. Each curve is labeled by the initial thickness of the film. The thickness removed by sputtering is indicated on the top axis.

D. Dependence of irradiation-induced stress on the initial thickness of the films

For the group of slightly tensile Pt films, we find that the stress evolution depends on the initial thickness of the films. This contrasts with the highly compressive films, for which the irradiation-induced stress is independent of the initial film thickness. Figure 5 shows the stress evolution of Pt films irradiated with 4 keV Ar. The films are grown at 200 °C, with a series of thicknesses ranging from 20 to 40 nm. The initial stresses in the films are slightly different; however, these differences are less than ≈0.1 GPa (Fig. 1) and therefore negligible. The stress evolution is observed to systematically vary as the film thickness increases from 20 to 40 nm. For the 20 nm film, the change in stress thickness turns into a tensile direction at relatively low doses ($\approx2.5\times10^{15}$ cm^{-2}). As the initial film thickness increases, the turning point in the stress-thickness curve shifts to a higher dose. For the 40 nm thick film, the stress thickness continues to decrease up to the highest dose that we used.

Since x-ray analysis shows that the microstructure for the 20 and 40 nm films is similar, the observed dependence can only be explained by the interaction of ion-induced damage with the Si substrate. For reference, the thickness of Pt removed by sputtering (estimated by SRIM) is shown in the top axis of Fig. 5. The range for 4 keV Ar in Pt is 3.4 nm (from SRIM). Even including the straggle of the ions and the thickness of the sputtered Pt, the ions are not expected to reach the Si substrate at the turning point on the curve. These results therefore support our earlier conclusion that the creation of compressive stress in the film extends to regions deeper than the range of the ions.

TABLE I. Relaxation volumes of various defects in units of atomic volumes Ω.

Type of defect	Relaxation volume per defect for initial stress =0 GPa	Relaxation volume per defect for initial stress =−1.3 GPa
Surface adatom	0.216	0.162
Surface vacancy	0.168	−0.036
Surface vacancy cluster (with 12 vacancies)	0.048	0.021
Interstitial	2.03	2.08
Bulk vacancy	−0.441	−0.441
Bulk interstitial loop (with five atoms)	1.75	1.76
Bulk vacancy loop (with nine vacancies)	−0.452	−0.463

IV. MOLECULAR DYNAMICS SIMULATIONS

To determine the microscopic mechanisms that induce the change in stress, we simulated the initial stages of the ion bombardment process by using MD simulations. The details of the MD simulations can be found in Ref. 29. Ar ions with energies from 1 to 4 keV were examined. The computational cell employed periodic boundaries in the x-y plane and free (111) surfaces in the z directions. The dimensions of the cell were $6.1\times 5.8\times 5.5\ \mathrm{nm}^3$ in the x-y-z directions, respectively. An embedded-atom method[31] potential was used to simulate the interactions between Pt atoms. For the interaction between the inert gas atom and Pt atom, the purely repulsive universal potential[32] was employed. The same MD code has been previously used to calculate the defect production in various metals during ion bombardment.[29,33]

During the irradiation, the cell was maintained at 300 K. In some simulations, a constant pressure is applied in the transverse directions to model the initial biaxial stress in our experimental samples. The cell was quenched to 10 K after 15 ps from the initial impact, and the number of defects was counted. The simulations therefore provide information on the initial damage produced by a single impact. While such modeling cannot completely follow the diffusional processes that defects undergo under prolonged irradiation, the aim here is to study how the different irradiation conditions affect the primary state of damage in the films and the short term annealing of the point defects.

Additional simulations were performed to determine the stress induced by different types of defects produced in the sample and to determine the effect of the stress on the diffusional properties of the defects. The defects include surface vacancies and adatoms, bulk vacancies and interstitials, and finally various clusters of defects. We begin by calculating the stress introduced into the film by the different defects.

A. Volumetric change induced by defects

In these simulations, a single defect or defect cluster is introduced into an otherwise perfect lattice, and the change in the average stress in the transverse direction of the cell and the effective relaxation volume of the defect are determined. The relaxation volumes per defect are listed in Table I, which are expressed in units of the atomic volume Ω. Two sets of cells with initial stress equal to 0 and −1.3 GPa are used. Bulk vacancy and interstitial clusters in the form of loops on the (111) plane with an orientation 70.5° away from surface normal were also considered.

These calculations show that bulk defects have larger relaxation volumes than surface defects. The magnitude of the relaxation volume of an interstitial is about five times larger than that of a vacancy. This difference is similar to the previous simulation results reported in Cu.[34] For a cluster in the bulk, the relaxation volume per defect is essentially constant for cluster sizes less than ten atoms. Furthermore, only bulk vacancies or vacancy clusters can induce a significant in-plane tensile stress. This is in contrast to a surface vacancy cluster, which yields a compressive stress. Finally, the relaxation volumes of the bulk defects are not sensitive to the initial stress of the cell, as expected from linear elasticity theory.

B. Number of surface and bulk defects induced by single impacts

Figure 6 shows the number of defects produced as a function of ion energy. The solid symbols and open symbols represent results taken from cells with an initial stress of −1.35 or +0.15 GPa, respectively, corresponding to the two types of Pt films used in the experiments. The defects are classified as adatoms, surface vacancies, bulk vacancies, and interstitials. Vacancies found in the first layer of atoms are considered surface vacancies. Each datum represents the average from 45 independent runs. Bulk defects are generally found as single defects and are not clustered. On the surface, however, a crater is usually formed at the impact point. Surface defects around the crater exist either individually or in the form of a cluster. Typical defect arrangements can be found in Refs. 29 and 33.

Figure 6 shows that the number of bulk defects (bulk vacancy and interstitials) approximately increases linearly with energy, but that the number of surface defects begins to saturate for energies larger than 2 keV. A similar trend in the

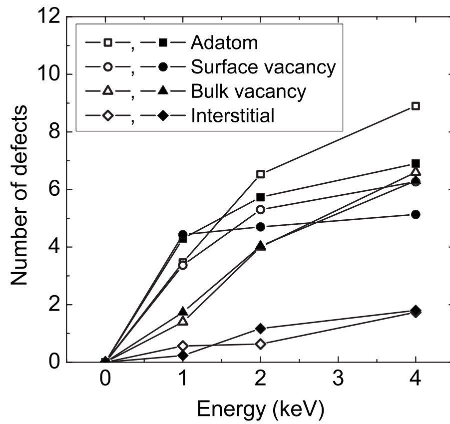

FIG. 6. MD simulation of the number of interstitials, bulk vacancy, surface vacancy, and adatom created by a single impact of Ar ion on a Pt(111) surface as a function of energy. The solid and open symbols represent the data taken with initial stresses of −1.35 and 0.15 GPa, respectively.

defect production yield was observed in earlier MD simulations.[35] Notably, the number of bulk defects does not strongly depend on the initial stress in the cell. This observation is perhaps not too surprising since the displacement energy to create a defect in Pt is ≈40 eV. These simulations thus clearly show that the experimental results cannot be explained by a difference in defect production in the two types of films. Similarly, the simulations show that the numbers of surface defects, adatoms, and vacancies also do not greatly vary with initial stress in the film. This too is not overly surprising since these defects arise from the thermal spike and a hydrostatic pressure of ≈1 GPa is small relative to the pressure developed during the thermal spike in Pt.

C. Effect of stress on the diffusion properties of interstitial atoms

Simulations were also performed to determine the effect of biaxial stress on the diffusion of interstitials atoms. We consider only interstitials since vacancies are not mobile in Pt at room temperature. Theoretical considerations of the effects of stress on the diffusion of interstitials can be found in the literature.[36] Biaxial stress on both the (100) and (111) planes were employed. Detailed accounts of the method for determining the diffusion constants by MD are presented elsewhere.[37] In Fig. 7, we show the results for the diffusion coefficients both in plane and normal to the applied stresses for biaxial stress applied on the (111) planes. A large anisotropy in the diffusion coefficient is clearly evident, with the out-of-plane diffusivity becoming larger than the in-plane diffusivity by a factor of 4 at −1.3 GPa.

While the experiments only employ (111) oriented films, we note that if the biaxial compressive stress is applied in the (100) planes, the in-plane diffusivity, which is in contrast to (111) films, becomes larger than the out-of-plane diffusivity, in this case by a factor of ≈10 by −2.0 GPa. The explanation for this behavior goes beyond the scope of this work, but it will be presented in a forthcoming article.[37] Here, we simply point out that the ratio of the diffusivity along the in-

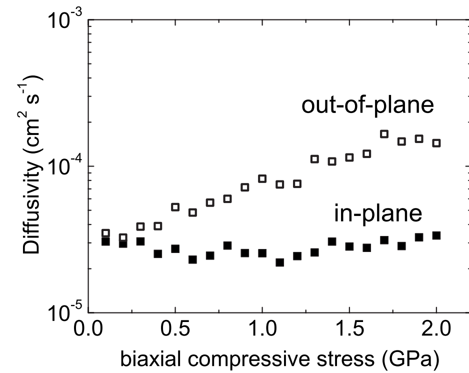

FIG. 7. The in-plane and out-of-plane diffusion constants of interstitials measured by MD simulations at 300 K. A biaxial compressive stress, which is varied from 0.1 to 2 GPa, is applied on the (111) planes. A small and constant compressive stress of 0.1 GPa is always maintained in the out-of-plane direction.

plane and the out-of-plane directions depends on the dipole strain of the interstitials at the saddle point as well as the orientation of the dipole tensor with respect to the lattice. A very different diffusion behavior can thus be obtained as the crystal orientation is changed with respect to the direction of the biaxial stress. We find, in fact, that the interstitial defect, which is normally a (100) dumbbell in Pt (and most fcc metals), begins to migrate as a (110) crowdion defect at biaxial stresses of ≈−1.5 GPa, which further causes the diffusion to be anisotropic.

V. DISCUSSION

The results in Sec. III show that the irradiation-induced stress sensitively depends on the mass of the ions, the initial stress in the Pt films, and the thickness of the films, indicating that several mechanisms are involved. Before accounting for each of these mechanisms, we point out that we find no significant differences in grain sizes determined by x-ray analysis in the samples that are grown at 200 °C or RT; moreover, no changes in grain size were observed during irradiation. We therefore neglect any possible effects of grain size in what follows.

A. Thermal spike and the creation of tensile stress

The behavior observed in the irradiated highly compressive Pt films is relatively simple. Except for He, an initially rapid rise in tensile stress is observed with ion dose, followed by a steady-state regime (Fig. 2), in which the change in stress is due to sputtering. The curves can be well characterized by two parameters: the initial slope for the tensile rise ($d\Delta S/d\Phi$) and a saturation dose Φ_0. In order to determine the mechanism causing this rapid rise, we consider how these two parameters depend on ion species and energy.

First, we relate the experimental observations to parameters that can be used to characterize the ion-induced damage. Assuming a biaxial stress state in the Pt thin film, the initial slope of the curve can be related to the total volume change induced by an impact through

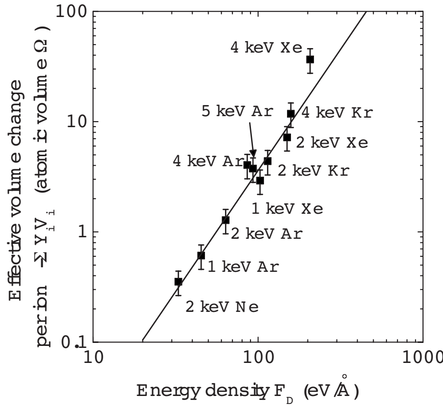

FIG. 8. The effective volume change induced per ion as a function of the energy deposition density of the ion. Note that all volume changes are negative (volume contraction). A negative sign is multiplied to the volumes so that we can present the data in a log-log plot. The volume change is calculated from the initial slope of the stress-thickness curves in Fig. 2 for the highly compressive films. The solid line on the graph is a fit to Eq. (4).

$$\left.\frac{\partial(\Delta S)}{\partial \Phi}\right|_{t=0} = -\frac{E_{\mathrm{Pt}}}{3(1-\nu_{\mathrm{Pt}})}\sum_i Y_i V_i. \quad (3)$$

In this equation, E_{Pt} and ν_{Pt} represents the elastic modulus and the Poisson ratio of Pt, respectively, Y_i is the yield of defect species i, and V_i is the relaxation volume of this type of defect. The summation on the right hand side represents the net volume changes contributed from all possible types of defects created in an impact. Equation (3) is valid in the initial stage of irradiation before the collision cascade overlaps with each other. By using Eq. (3), we can convert the initial slope to the average net volume change induced by an individual ion.

To gain further insight into the type of defects that dominate the summation, we turn to the results from our MD simulations. First, Table I shows that the stress generated by bulk defects is a few times to an order of magnitude larger than their surface counterparts. Furthermore, surface defects are mobile at RT.[38] Recombination and clustering can occur, which will reduce the stress contributed by the surface defects. We therefore assume that most of the change in stress derives from bulk defects. Furthermore, since the observed change in stress is in the tensile direction, this change must be due to bulk vacancies and their clusters.

During an ion impact, local heating in the cascades causes materials around the ion track to melt. For most metals, including Pt, the specific volume of the melt is larger than that of the solid, and some of the atoms in the cascades will therefore flow onto the surface. Upon solidification, atoms that have flowed onto the surface become adatoms and the missing mass below the surface condenses out as vacancies (Fig. 6). This process has been illustrated in previous MD simulations,[33] as well as experimentally.[38] The number of bulk vacancies formed is proportional to the amount of materials that flows to the surface during melting, assuming for now that the number of bulk interstitials is negligible in this case. If we next approximate the cascade shape by a cylindrical spike around a straight ion track, the total number of atoms that move to the surface can be shown to be proportional to F_D^2,[39] where F_D is the energy density deposited by the ion. To test our result with the thermal spike model, we plot the net volume change (in units of atomic volume of Pt) calculated by Eq. (3) against F_D determined by SRIM for different ions (see Fig. 8). The straight line in this log-log plot is a fit to

$$-\sum_i Y_i V_i = A F_D^n, \quad (4)$$

where A and n are fitting constants. We find $n=2.2\pm0.2$, which is very close to the prediction of the thermal spike model ($n=2$).[40] In addition, for 2 keV Ar, we found that the total relaxation volume is 1.3 Ω. In the MD simulation, we calculated that ≈4 bulk vacancies and ≈1 interstitial atom are formed per incident of 2 keV Ar atom. If we assume that most interstitials annihilate at surface or vacancies and use the calculated relaxation volume of a vacancy (Table I), 0.44 Ω, we find good agreement between the experiments and simulations.

If the tensile rise in the early stage is created by the thermal spike, the saturation dose can be related to the dose when spikes begin to overlap. This is because bulk vacancies in Pt are immobile at RT[28] and therefore cannot diffuse away from the position where they are formed. A vacancy can only be annihilated when it falls into the melting zone of another ion. For a spike of radius r, the saturation dose $\Phi_{0,\mathrm{sp}}$ will be approximately equal to $1/\pi r^2$. The radius can be approximated from SRIM simulation, which gives $r\sim1.2$ nm for 2 keV Ar. This gives $\Phi_{0,\mathrm{sp}}\sim2.2\times10^{13}$ cm^{-2}. On the other hand, the saturation dose determined from experiments (Fig. 2) is 1.1×10^{14} cm^{-2}. The reason for the discrepancy between the experimental data and this simple estimation is uncertain, but it is known that as the liquid zone refreezes, vacancies are swept toward the center of the cascade, and this essentially reduces r (Ref. 2). It is also possible, however, that vacancies continue to build up in the same region until a few exposures to the melting zone.

B. Role of anisotropic diffusion of ion-induced interstitials

In Sec. V A, we have considered the flow of mass onto the surface as the source of tensile stress in irradiated thin films. We did not consider the interstitial atoms even though the simulations show that the product of their number and relaxation volume exceeds that same product for any of the other types of defects, including vacancies. We tacitly assumed, therefore, that since the interstitials are mobile, they recombined with vacancies or migrated to sinks, presumably the surface. Since the number of bulk vacancies well exceeds the number of interstitials, recombination always increases the ratio of vacancies to interstitials and increases the tensile stress. While this explanation satisfactorily explains our experiments on Pt thin films initially under compressive stress, we are still left to explain the surprising result that films initially under slightly tensile stress behave nearly opposite to those initially under compressive stress; i.e., they become compressive under irradiation. Since the defect production

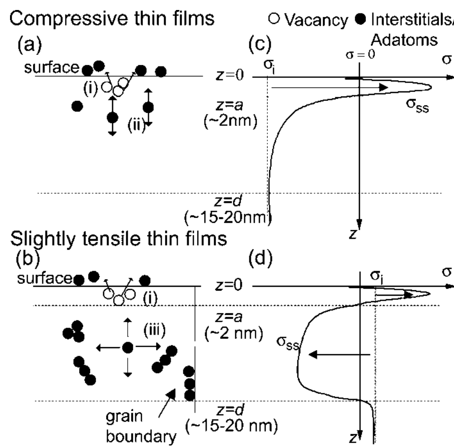

FIG. 9. Atomistic processes occur in the surface region during ion bombardment. (a) In a film with a strong initial compressive stress, (i) the thermal spike process induce tensile stress within the implantation depth of the ion ($0<z<a$); (ii) the interstitials have a bias to diffuse in the out-of-plane direction, which leads to recombination with vacancies or loss at the free surface. (b) In a film with a slightly tensile stress, (iii) interstitials can diffuse in the lateral direction as well, which leads to the creation of interstitials loops and attachment of interstitials to the grain boundary. These processes create compressive stress in the region ($a<z<d$) beyond the ion implantation depth. [(c) and (d)] Schematics show the stress evolution in the two group of films, from initial state (σ_i, dotted lines) to the steady state (σ_{ss}, solid lines). The arrows between the profiles indicate the direction of stress change. At the steady state, a stress gradient is present that suppresses the further incorporation of interstitials.

was shown to be nearly independent of the initial state of stress, we must conclude that the interstitials are not as efficiently lost at the surface or to recombination in the absence of the biaxial compressive state of stress. We now illustrate how this is possible.

In Fig. 9, we schematically show the evolution of the damage state following a particular impact event. Vacancies are shown closer to the surface than the interstitials, as found in MD simulations. As discussed in Sec. IV C, the diffusion of interstitials is strongly anisotropic with regard to in-plane and out-of-plane directions if an external biaxial stress is applied. With an initial compressive stress of ~1 GPa, the out-of-plane diffusivity of interstitials is three to four times larger than the in-plane diffusivity. This directs interstitials to diffuse preferentially normal to the plane of the surface and the interstitials will be predominantly lost by recombination with vacancies near the surface or the surface sink [Fig. 9(a)]. In the absence of stress, on the other hand, interstitials can migrate parallel to the surface and find other mobile interstitials and immobile interstitial clusters. Interstitials near grain boundaries can incorporate into them as well [Fig. 9(b)]. These processes all create compressive stress at a depth beyond the implantation depth of the ions. To explain the initial rate of increase of integrated stress, for example, for the 2 keV Ar irradiation, we only need an addition of 0.7 interstitials per ion from immobile clusters for the slightly tensile films. Similar ideas of anisotropic diffusion have been commonly employed to explain irradiation-induced creep[41] and diffusion of dopants in semiconductor materials.[42]

With the above picture, we can construct the steady-state stress as a function of depth, as schematically shown in Figs. 9(c) and 9(d). The steady-state is referred to as the instance when all the stress-creating mechanisms are saturated. In both types of films, the surface region is relatively tensile because of the vacancy loops created inside the thermal spike. For the slightly tensile film, interstitials start to cluster deeper in the film, as the vacancy loops are forming, and develop a compressive layer below the tensile layer. In this way, the stress states in the two films become similar, although the source of the compression in these films is different. We point out that as interstitials cluster in the initially tensile film and generate compressive stress, a gradient in the stress state also develops. This gradient in stress will bias interstitial migration toward the surface. Together this stress and the increasing diffusion anisotropy lead to saturation in the compressive stress.

The above picture explains the experimental results shown in Fig. 4 for initially tensile films. The initial tensile peak observed is due to the thermal spikes, which is more pronounced for bombardment with Xe ions than Ar ions. The same trend is observed in the highly compressive films (Figs. 2 and 8), in which stronger tensile rise is associated with the higher ion stopping power. As the ion dose increases, more interstitials incorporate into the film and the change in total stress thickness eventually turns compressive. For lower-energy or lighter ions (e.g., 2 keV Ar), the interstitial mechanism dominates the process and only compressive stress is observed.

We next turn to the depth of the damage zone. In Fig. 3, we found recovery in the stress state when we switch from high-energy ions to low-energy ions, even though the lower-energy ions cannot reach the entire damaging zone created by the higher-energy ions. This can of course be explained by recognizing that interstitials are mobile at room temperature and so they can migrate from shallow depths after creation by low-energy ions to preexisting deeper vacancies produced earlier by higher-energy recoils. It is possible too that the same thermal spike mechanism that forces atoms to flow onto the surface can also force mass deeper to vacancy rich regions. In either case, damage created by low-energy ions can remove the tensile damage created by higher-energy ions. This results in the "reversibility" observed in the stress evolution when we switch between different ion energy. In addition, the dose needed for the stress to recover is about five times larger than the dose for the tensile stress to be created by the 4 keV ions. This observation can be explained by the lower defect yield of the 1 keV ions.

In this same regard, we have pointed out in Sec. III C that the apparent film stress for the slightly tensile film bombarded by 2 keV Ar is unphysically high (6 GPa) if we were to assume that all of the compressive stress is created within the range of the ions. The amount of stress becomes more reasonable, on the other hand, when we assume that the compressive stress is actually distributed in a much wider region across the film. For example, if we take the diffusion range of interstitials to be 15 nm, the steady-state stress in the compressive layer will be ~1 GPa, instead of the high value previously calculated.

We can estimate the maximum range of interstitials from the dependence of the irradiation-induced stress on the initial thickness of the film. Figure 5 shows that the total stress thickness reaches a minimum and then turns tensile for the 20 and 25 nm thick Pt films. Less compressive stress is developed in the thinner film because the number of interstitials that can be accumulated in a thinner film is less. Moreover, the sputter process decreases the film thickness as a function of time. Hence, the turnover in the curve at a higher dose can be explained by removal of the compressive layer built up early in the irradiation by continuous sputtering. We estimate the diffusion range of interstitials before they reach a sink by looking at the 25 nm curve. The stress thickness starts to peak after 4 nm of materials is removed. Assuming at this dose the interstitials begin interacting with the underlying substrate and accounting for the range of the 4 keV Ar ($\sim$3–5 nm), the interstitial can travel as far as 15–20 nm beyond the cascade; this is comparable to the grain size of the film.

C. Stress induced by He irradiation

Due to the very low ratio of projectile to target mass, the damage in Pt created by He ions is much different from the damage created by other noble gas ions. SRIM simulation shows that a He ion with energy less than 1 keV produces few Frankel pairs (less than 10^{-4} per ion) by direct collision. Therefore, the stress is not likely to be caused by the ion-induced defects, as described in Secs. V A and V B. From our experimental results, compressive stress is produced in both groups of Pt films despite their different initial states of stress. For the compressive films, however, the stress saturates at relatively low dose ($\sim 5\times10^{15}$ cm^{-2}), with only a small increase in total stress ($\sim$0.3 GPa, assuming the stress distributed uniformly on the top 15 nm of film), while the tensile films become increasingly compressive for doses as high as 2×10^{16} cm^{-2} (not shown in Fig. 4). Here, the compressive stress increases by $\sim$1.2 GPa, which is still $\sim$0.5 GPa less than the total stress in the initially compressive film.

Since the defect yield is negligible, He ions must play a role in inducing the observed compressive stress. It is known that gas bubbles and interstitial loops can be formed in metals irradiated by He and H ions.[43–45] Transmission electron microscope (TEM) studies show that interstitial loops can be formed in W by He ions with energies as low as 0.5 keV.[43] The production of interstitials is triggered by high pressure, He-vacancy complexes.[43,45] The He-vacancy complexes are not likely to create a significant amount of stress, but the interstitial loops can create large compressive stress. Similar to the interstitial mechanism discussed in Sec. V B, the loops can be formed at a distance beyond the ion implantation depth, which is also directly observed by TEM studies.[43]

To provide an approximation on the stress that can be created by these interstitial loops, we use the data reported in Ref. 43 on the irradiation of W by 0.5 keV He ions. In their studies, the atomic fraction of defects is around 5×10^{-3} at a dose of 5×10^{15} cm^{-2}, which is distributed evenly across the top 15 nm of the sample. Since interstitials are in the form of loops, this number should roughly equal to the volumetric strain in the crystal. We assume that a similar defect density is present in the Pt film bombarded by 0.5 keV He. The stress can be calculated by using the elastic constant for Pt and is equal to 0.62 GPa. The stress in the Pt irradiated with 0.5 keV He (Fig. 4) can be calculated by assuming that the stress uniformly distributes across the top 15 nm of the film. The change in stress thickness at $\Phi=5\times10^{15}$ cm^{-2} is 8 N m^{-1}, which corresponds to a stress of 0.53 GPa. Therefore, the creation of interstitial loops can reasonably account for the amount of stress we observed in the irradiation experiment.

Finally, a saturation dose larger than 2×10^{16} cm^{-2} is observed for the slightly tensile Pt film. This is again consistent to the TEM studies in Ref. 43, which shows that the number of loops does not saturate until a dose of 10^{17} cm^{-2}. Physically, He ions create many fewer defects per ion than other noble gas ions, which increases the saturation dose. For our highly compressive Pt film, the stress saturates at a much lower dose. This can be due to that fact that the high compressive stress in the film prohibits the development of the interstitial loop or the film starts to yield at this high compressive stress.

VI. CONCLUSION

The stress induced in Pt thin films by irradiation of inert gas ions can either be tensile or compressive, depending on the initial film stress and the mass of the ions. The complexity of the experimental results illustrate that various kinetic process are at play. In this work, we demonstrate for heavy inert gas ions that two major mechanisms contribute to the observed stress change, tensile stress by the melting along the ion track and compressive stress by the incorporation of interstitials into the film. The latter mechanism involves interstitial diffusion, which can create stress beyond the ion range. By varying the initial stress of the film or the mass of the ions, individual mechanisms can be enhanced or suppressed, which results in the wide range of observed behaviors. The thermal spike mechanism can be enhanced by an increase in ion mass or energy. The interstitial mechanism, on the other hand, can be suppressed in (111) oriented films by applying an in-plane biaxial compressive stress.

MD simulations have revealed that the dependence of irradiation-induced stress on the initial stress in the film derives from anisotropic interstitial diffusion in a uniform biaxial stress field. This anisotropy controls the final attachment sites for these highly mobile defects. In an initially compressive film, interstitials diffuse faster in the out-of-plane direction, which makes them preferentially annihilate at the surface, or with vacancies near the surface instead of nucleating loops inside the bulk. In addition, a stress gradient developed in the film during irradiation may also enhance this preferential attachment at a later stage of irradiation.

The present work also shows that low-energy He irradiation, unlike the other inert gases, always leads to additional compressive stress in Pt thin films. We attribute this difference to the light mass of He since at the energies employed, He cannot efficiently produce point defects in Pt by recoil events. As a consequence, He traps at either defect sites or

grain boundaries and adds compressive stress. It is also possible that He forms small bubbles and "punches out" interstitial loops, additionally adding to the compressive stress.

ACKNOWLEDGMENTS

We are thankful to P. Ehrhart for the useful discussions on the properties of point defects under a stress field. This work is supported by the U.S. National Science Foundation under Grant No. DMR-0419840 and in part by the U.S. Department of Energy, Basic energy Sciences under Grant No. DEFG02-05ER46217. Part of the experimental works was carried out in the Center for Microanalysis of Materials, University of Illinois, which is partially supported by the U.S. Department of Energy under Grant No. DEFG02-91-ER45439.

[1] E. Chason, S. T. Picraux, J. M. Poate, J. O. Borland, M. T. Current, T. D. de la Rubia, D. J. Eaglesham, O. W. Holland, M. E. Law, C. W. Magee, J. W. Mayer, J. Melngailis, and A. F. Tasch, J. Appl. Phys. **81**, 6513 (1997).
[2] R. S. Averback and T. Diaz de la Rubia, in *Solid State Physics*, edited by H. Ehrenreich and F. Spaepen (Academic, New York, 1998), Vol. 51, p. 281.
[3] P. Sigmund, in *Sputtering by Particle Bombardment*, edited by R. Behrisch (Springer-Verlag, Berlin, 1981), Vol. 1, pp. 9–71.
[4] W. L. Chan and E. Chason, J. Appl. Phys. **101**, 121301 (2007).
[5] K. Zhao, R. S. Averback, and D. G. Cahill, Appl. Phys. Lett. **89**, 053103 (2006); X. Hu, D. G. Cahill, and R. S. Averback, *ibid.* **76**, 3215 (2000).
[6] R. A. Enrique and P. Bellon, Phys. Rev. Lett. **84**, 2885 (2000).
[7] V. B. Shenoy, W. L. Chan, and E. Chason, Phys. Rev. Lett. **98**, 256101 (2007).
[8] J. Stangl, V. Holy, and G. Bauer, Rev. Mod. Phys. **76**, 725 (2004).
[9] G. Ozaydin, K. F. Ludwig, H. Zhou, and R. L. Headrick (unpublished).
[10] H. B. George, B. Davidovitch, M. P. Brenner, and M. J. Aziz (unpublished).
[11] N. V. Medhekar, V. B. Shenoy, W. L. Chan, and E. Chason (unpublished).
[12] T. G. Bifano, H. T. Johnson, P. Bierden, and R. J. Mali, J. Microelectromech. Syst. **11**, 592 (2002).
[13] C. A. Volkert, J. Appl. Phys. **70**, 3521 (1991).
[14] E. Snoeks, A. Polman, and C. A. Volkert, Appl. Phys. Lett. **65**, 2487 (1994).
[15] H. Trinkaus and A. I. Ryazanov, Phys. Rev. Lett. **74**, 5072 (1995).
[16] E. Snoeks, T. Weber, A. Cacclato, and A. Polman, J. Appl. Phys. **78**, 4723 (1995).
[17] M. L. Brongersma, E. Snokes, and A. Polman, Appl. Phys. Lett. **71**, 1628 (1997).
[18] S. G. Mayr and R. S. Averback, Phys. Rev. B **68**, 214105 (2003).
[19] N. Kalyanasundaram, M. C. Moore, J. B. Freund, and H. T. Johnson, Acta Mater. **54**, 483 (2006).
[20] K. Zhao, D. G. Cahill, and R. S. Averback (unpublished).
[21] K. Dahmen, M. Giesen, J. Ikonomov, K. Starbova, and H. Ibach, Thin Solid Films **428**, 6 (2003).
[22] W. L. Chan, E. Chason, and C. Iamsumang, Nucl. Instrum. Methods Phys. Res. B **257**, 428 (2007).
[23] C. A. Crider, J. M. Poate, J. E. Rowe, and T. T. Sheng, J. Appl. Phys. **52**, 2860 (1981).
[24] X. J. Zhang and D. G. Cahill, Langmuir **22**, 9062 (2006).
[25] G. G. Stoney, Proc. R. Soc. London, Ser. A **82**, 172 (1909).
[26] H. Windischmann, Crit. Rev. Solid State Mater. Sci. **17**, 547 (1992).
[27] J. F. Ziegler and J. P. Biersack, SRIM-2000.40, IBM, Yorktown, NY, 1984.
[28] R. W. Balluffi, J. Nucl. Mater. **69-70**, 240 (1978).
[29] K. Nordlund, M. Ghaly, R. S. Averback, M. Caturla, T. Diaz de la Rubia, and J. Tarus, Phys. Rev. B **57**, 7556 (1998).
[30] J. K. Mason, A. C. Lund, and C. A. Schuh, Phys. Rev. B **73**, 054102 (2006).
[31] S. M. Foiles, M. S. Daw, and M. I. Baskes, Phys. Rev. B **33**, 7983 (1986).
[32] J. F. Ziegler, J. P. Biersack, and U. Littmark, *The Stopping and Range of Ions in Matter* (Pergamon, New York, 1985).
[33] M. Ghaly, K. Nordlund, and R. S. Averback, Philos. Mag. A **79**, 795 (1999).
[34] P. H. Dederichs, C. Lehmann, H. R. Schober, A. Scholz, and R. Zeller, J. Nucl. Mater. **69-70**, 176 (1978).
[35] H. Gades and H. M. Urbassek, Phys. Rev. B **50**, 11167 (1994).
[36] P. H. Dederichs and K. Schroeder, Phys. Rev. B **17**, 2524 (1978).
[37] W. L. Chan, Y. Ashkenazy, and R. S. Averback (unpublished).
[38] M. Morgenstern, T. Michely, and G. Cosma, Philos. Mag. A **79**, 775 (1999).
[39] R. S. Averback and M. Ghaly, J. Appl. Phys. **76**, 3908 (1994).
[40] Note that a continuous cylindrical spike along the ion track is assumed in the model in (Ref. 39). For the low-energy ions used in our experiments, the real shape of the spike can derivate significantly from this ideal shape.
[41] C. H. Woo, J. Nucl. Mater. **120**, 55 (1984).
[42] M. J. Aziz, Y. Zhao, H.-J. Gossmann, S. Mitha, S. P. Smith, and D. Schiferl, Phys. Rev. B **73**, 054101 (2006).
[43] N. Yoshida, E. Kuramoto, and K. Kitajima, J. Nucl. Mater. **103**, 373 (1981).
[44] S. E. Donnelly, R. C. Birtcher, C. Templier, and V. Vishnyako, Phys. Rev. B **52**, 3970 (1995).
[45] Y. Watanabe, H. Iwakiri, N. Yoshida, K. Morishita, and A. Kohyama, Nucl. Instrum. Methods Phys. Res. B **255**, 32 (2007).